RI 8455

Bureau of Mines Report of Investigations/1980

NEWARK PUBLIC LIBRARY

NOV 14 1980

U.S. GOVT. PUBS.
DEPOSITORY 376

Characterization of Thin Films and Solid Surfaces Using Proton-Induced X-Ray Emission

By Bruce D. Sartwell and Arthur B. Campbell III

UNITED STATES DEPARTMENT OF THE INTERIOR

I28.23:

Report of Investigations 8455

Characterization of Thin Films and Solid Surfaces Using Proton-Induced X-Ray Emission

By Bruce D. Sartwell and Arthur B. Campbell III

UNITED STATES DEPARTMENT OF THE INTERIOR
Cecil D. Andrus, Secretary

BUREAU OF MINES
Lindsay D. Norman, Acting Director

best copy available

This publication has been cataloged as follows:

Sartwell, Bruce D

Characterization of thin films and solid surfaces using proton-induced X-ray emission.

(Report of investigations • Bureau of Mines ; 8455)
Bibliography: p. 21-22.
Supt. of Docs. no.: I 28.23:8455.

1. Thin films, Effect of radiation on. 2. Solids—Surfaces. I. Campbell, Arthur B. III 1943- joint author. II. Title. III. Series: United States. Bureau of Mines. Report of investigations ; 8455.

TN23.U43 [QC176.84.R3] 622s [530.4'1] 79-607938

CONTENTS

	Page
Abstract	1
Introduction	1
Experimental work	2
Theory and applications	4
Results and discussion	10
Cross sections and calibration measurements	10
Thin-film analysis	14
Bulk analysis	15
Depth profiling	18
Summary and conclusions	19
References	21

ILLUSTRATIONS

1.	Schematic of ultra-high-vacuum target chamber in which the PIXE analyses were conducted	3
2.	Plot of the oxygen K X-ray yield $I(E_o)$ as a function of Fe_3O_4 film thickness	7
3.	Plot of the equivalent surface coverage of carbon determined by PIXE as a function of the actual bulk carbon impurity concentration	9
4.	Correction factors used in the normalization of individual X-ray yields to obtain atomic percent concentration for bulk analysis	9
5.	X-ray production cross sections for K-shell, L-shell, and M-shell excitation by protons	11
6.	Plot of the iron L X-ray yield as a function of iron film thickness	12
7.	Oxide thickness plotted as a function of exposure time for iron and three ion-implanted iron samples	13
8.	Oxidation kinetics of high-purity iron for two different initial sulfur surface coverages	15
9.	Integral distribution and depth profiles as determined by the PIXE-sputtering technique for 25-kev Ni^+ implantation into iron	17
10.	Platinum M and iron K experimental X-ray yields for 150-kev proton bombardment as a function of sputtering charge for an electrodeposited platinum film	19

TABLES

1.	Thickness of oxide film measured using three different proton-beam angles of incidence	5
2.	Ratio of the substrate aluminum K yields obtained before and after evaporation as compared to the ratio predicted from the evaporated iron film thickness measured using the thin-film and integral approximations	13
3.	PIXE results for the A-286 turbine wheel	16
4.	PIXE results for the Nimonic-105 turbine blade	17

CHARACTERIZATION OF THIN FILMS AND SOLID SURFACES USING PROTON-INDUCED X-RAY EMISSION

by

Bruce D. Sartwell[1] and Arthur B. Campbell III[2]

ABSTRACT

The Bureau of Mines is using characteristic X-rays produced by proton bombardment of a solid surface to provide quantitative compositional analyses of surface layers of metals. An integral X-ray yield equation has been developed that quantitatively relates the measured X-ray yield to the thickness of thin films ranging from less than a monolayer to several thousand angstroms. The use of the integral yield equation is demonstrated for the growth of a thin film by vacuum evaporation. Results are presented that show how proton-induced X-ray emission (PIXE) has been used to determine the oxidation kinetics of iron that had been implanted with several different species of heavy ions. The sensitivity of PIXE for the measurement of very-thin-film growth kinetics is demonstrated from studies of the effect of fractional monolayer coverages of sulfur on the initial oxidation kinetics of iron. Results are also presented in which PIXE has been used to study the redistribution of alloying elements in components of a gas turbine that had fractured due to corrosion fatigue. By combining PIXE with low-energy ion sputtering, quantitative composition depth profiles of surface layers are obtained. Examples are presented for the profiling of iron samples implanted with 25-kev nickel ions and for a platinum coating on an Fe-5Cr substrate.

INTRODUCTION

A principal objective of the Bureau of Mines is to conserve the Nation's mineral resources. In keeping with this goal, the Bureau's Avondale Research Center has been conducting studies to determine the mechanisms responsible for the oxidation and corrosion of metallic materials that can be used in metallurgical processing operations and thus increase the useful life of materials in process components. Although metallic corrosion has been extensively studied for many decades, it was not until the early 1970's that the powerful techniques of surface science began to be fully utilized in this area.

[1]Research physicist, Avondale Research Center, Bureau of Mines, Avondale, Md.
[2]Formerly research physicist, Avondale Research Center, Bureau of Mines. Avondale, Md., now with Naval Research Laboratory, Washington, D.C.

READEX FICHE

Metallic corrosion can be defined as the interaction of a metal surface with its environment. In many cases, the initiation of a corrosion process involves the adsorption of a layer of a foreign specie on the metal surface, with subsequent chemical combination and then growth of a thin film. In alloys containing two or more metals, different chemical free energies for the formation of oxides can result in the depletion of a particular element or elements at the film-metal interface. This can also result in the formation of a protective oxide film by the element with the most negative free energy of formation. The final phase of corrosion can involve the formation of thick corrosion products resulting in changes in the substrate alloy composition over a significant depth. Therefore, a general study of corrosion processes should include (1) surface analyses that include only the first few atomic layers and are sensitive to small fractions of an atomic layer, (2) thin-film and thick-film analyses, and (3) substrate bulk analyses.

In this paper, the use of proton-induced X-ray emission (PIXE) in each of these three areas will be demonstrated. The emphasis will be on presenting illustrative examples rather than on detailed interpretive analyses of the results. These examples will include (1) monitoring the thickness of vacuum-evaporated films, (2) determining the oxide film growth kinetics for iron and for iron that has been implanted with 25-kev Fe^+, Ar^+, or Cr^+, (3) determining the effects of different sulfur surface coverages on the initial oxidation kinetics of iron, (4) determining the redistribution of alloying elements in superalloy turbine components subjected to corrosion fatigue, and (5) obtaining composition depth profiles of ion-implanted iron samples and electrodeposited platinum coatings.

EXPERIMENTAL WORK

The PIXE analyses described in this paper were accomplished using proton beams within an energy range of 100 to 200 kev that were obtained from a Cockroft-Walton electrostatic accelerator equipped with a radio-frequency ion source. The ion beam was mass-analyzed to separate the proton beam from the molecular hydrogen ion beam. The ultra-high-vacuum chamber in which the PIXE analyses were performed, shown schematically in figure 1, had a base pressure 1×10^{-9} torr; for most measurements reported here, the pressure in the chamber ranged from 4 to 8×10^{-8} torr. The proton beam was collimated to 0.2-cm diameter by apertures S_1 and S_2 with aperture S_3 biased for secondary electron suppression. The characteristic X-rays emitted from the sample were detected using two types of detectors: a gas-flow proportional counter containing a 90% argon-10% methane gas mixture and having two 2-μm-thick aluminized mylar entrance windows W_1 and W_2; and a Si(Li) solid state detector with 2-μm-thick aluminized Mylar and 25.0-μm-thick beryllium entrance windows, W_3 and W_4, respectively. The proportional counter was used only for detecting the very low energy C K and O K X-rays in order to determine surface carbon coverages and oxide film thicknesses. The solid state detector was used to measure all other elements. Due to attenuation in the beryllium window, X-rays with an

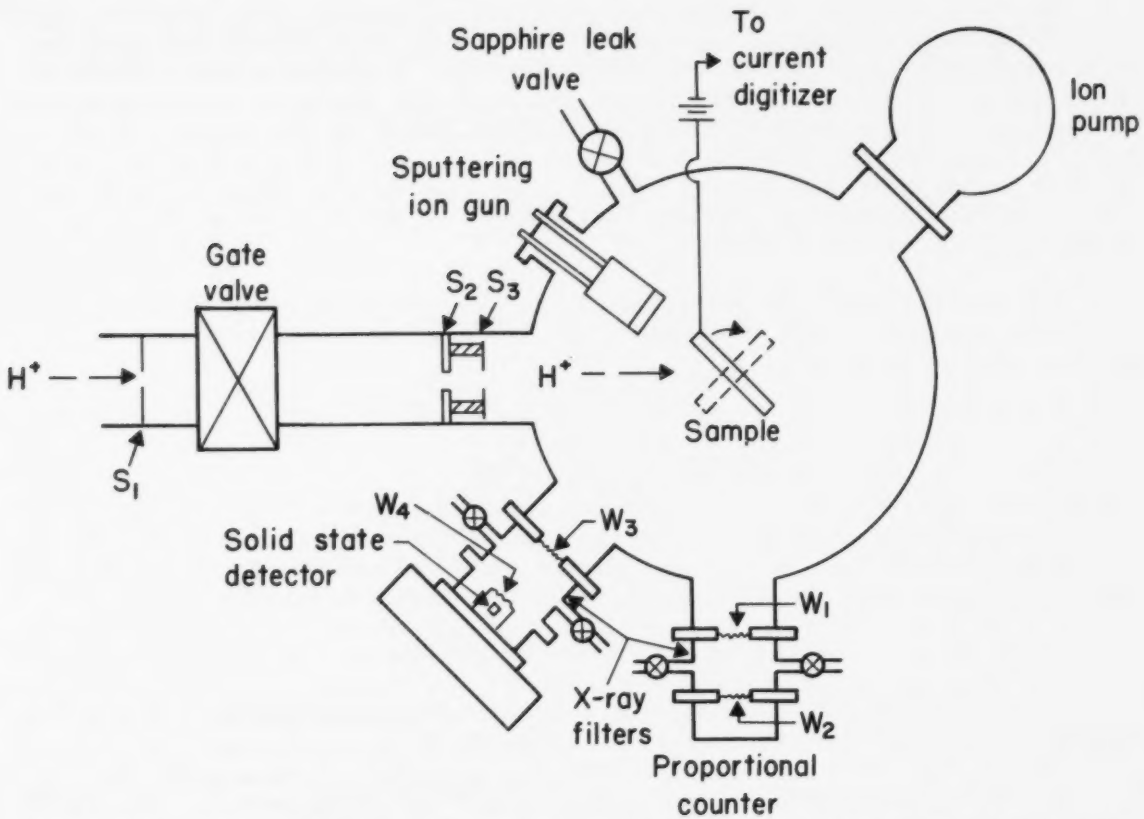

FIGURE 1. - Schematic of ultra-high-vacuum target chamber in which the PIXE analyses were conducted.

energy less than 0.8 kev could not be detected. The Si(Li) detector's cross-sectional area was 80 mm^2 and it had a resolution of 210 ev for Mn Kα X-rays. The X-ray filter attached to the proportional counter was utilized in the oxide film thickness measurements with high-purity oxygen being bled into the filter to a pressure of 100 torr. The oxygen attenuated the interfering C K and Fe L X-ray lines to a much greater degree than the O K X-rays and, therefore, permitted very sensitive measurements of surface oxygen. For all measurements made with the Si(Li) detector, the X-ray filter was maintained under vacuum.

The sputter ion gun was used in the depth-profiling studies. The procedure used for sputtering was to inject ultra-high-purity argon into the chamber to a pressure of 5×10^{-5} torr and then bombard the sample with 1.0-kev Ar^+ at normal incidence for a preselected amount of charge as determined by a digital current integrator. Also shown in figure 1 is a sapphire leak valve which was used for injecting either ultra-high-purity argon (for sputtering) or oxygen (for oxidation studies) into the chamber.

The X-ray spectra, obtained from analyses of samples, were accumulated in a multichannel pulse height analyzer (PHA). Proton beam current was measured on the sample using a digital current integrator. A preset scaler, connected to the output of the integrator, gated the PHA; this provided for preselection of the amount of proton beam charge to be accumulated on the target. Each peak in the X-ray spectrum was integrated and, following correction for background, the experimental X-ray yield, Y, expressed as the number of detected characteristic X-rays per incident microcoulomb of proton beam charge, was calculated.

The factor Y could be converted to the absolute X-ray yield $I(E_o)$, where E_o is the incident proton beam energy and $I(E_o)$ is expressed as X-rays per proton, using the equation (7)[3]

$$I(E_o) = \frac{4\pi(1.6 \times 10^{-13})Y}{(\lambda)(d\Omega)}, \qquad (1)$$

where $d\Omega$ is the solid angle subtended by the detector and λ is the detector efficiency which is determined from the transmission of the X-rays through the entrance windows of the detectors and, for the Si(Li) detector, the transmission of the X-rays through the silicon dead layer on the detector.

THEORY AND APPLICATIONS

The excitation of characteristic X-rays by proton bombardment of a solid material is generally described by the equation (4)

$$I(E_o) = n\int_0^{R_o} \sigma_x[E(E_o,r)]\exp(-\mu r)dr, \qquad (2)$$

where n is the number of target atoms/g, R_o is the total projected range of the protons in g/cm^2, $\sigma_x[E(E_o,r)]$ is the X-ray production cross section in cm^2/atom for protons with instantaneous energy E at a distance r in g/cm^2 along the projected proton path, and μ is the absorption coefficient in cm^2/g for the characteristic X-ray in the target material. If the element being detected is present as a surface film of thickness T, then equation 2 can be rewritten with a change of variable from the projected proton path length, r, to a depth x in cm normal to the sample surface,

$$I(E_o) = N_o \int_0^{T/\cos\theta} \sigma_x[E(E_o,x/\cos\theta]\exp(-\mu\rho\, x/\cos\theta)d(x/\cos\theta), \qquad (3)$$

where θ is both the angle between the incident proton beam and the sample normal and the angle between the detector and the sample normal, N_o is the atomic density of the film in atoms/cm^3, and ρ is the bulk density of the film in g/cm^3.

---

[3]Underlined numbers in parentheses refer to items in the list of references at the end of this report.

If a film is sufficiently thin such that the energy loss of the protons can be neglected, σ_x is a constant and equation 3 can be integrated to give

$$I(E_o) = N_o \sigma_x[E_o]\left\{\frac{1 - \exp(-\mu\rho\, T/\cos\theta)}{\mu\rho}\right\} \tag{4}$$

In addition, if the film is thin enough that absorption of the X-rays is negligible, the exponential in equation 4 can be expanded in a Taylor series to give

$$1 - \exp(-\mu\rho T/\cos\theta) \simeq \mu\rho T/\cos\theta \tag{5}$$

and

$$I(E_o) = N_o \sigma_x[E_o](T/\cos\theta) \tag{6}$$

or

$$T = \frac{I(E_o)\cos\theta}{N_o \sigma_x[E_o]} \tag{7}$$

The cos θ term takes into account the increase in X-ray yield for increased angles of incidence of the proton beam for a given film thickness T. If normally incident protons are used, then the cos θ term drops out. Previously published reports (3, 5) on measuring thin films, where non-normally incident protons were used, did not include the cos θ term in the thin-film equation (equation 7). To determine if the use of the cos θ term was correct, the thickness of an oxide film grown at 300° C on polycrystalline iron was calculated using equation 7 from measurements of the O K X-ray line obtained for three different values of the angle θ, 45°, 36°, and 18°. The results are summarized in table 1. From these measurements, it was concluded that the cos θ term must be included in the thin-film equation when non-normally incident protons are used.

TABLE 1. - Thickness of oxide film measured using three different proton-beam angles of incidence

θ, deg	Oxide thickness, A	
	Neglecting cos θ	Including cos θ
18.....	123	117
36.....	146	118
45.....	159	113

For films thick enough that equation 7 cannot be used, because the incident protons lose an appreciable amount of energy and/or the attenuation of the X-rays within the film is significant, equation 2 can be used with suitable approximations for the depth dependence of the X-ray production cross section and the X-ray attenuation coefficient. As an example, consider the case of an Fe_3O_4 film on an iron substrate. Using the thick-target O K X-ray production cross sections obtained by Hart (5) for proton energies between 20 and 100 kev, σ_x can be approximated by the function

$$\sigma_x \simeq (1.598 \times 10^{-29})E^{3.34}. \tag{8}$$

where E is the proton energy. This function was found to fit Hart's data with a statistical index of determination of 99.7%. To determine σ_x as a function of depth of penetration of the protons, it was necessary to calculate the average stopping power, de/dr' of the protons in the iron oxide. For an incident proton energy of 120 kev, equation 8 predicts that σ_x will be reduced to 10% of its initial value when E = 60 kev. From the stopping power data of Andersen (2), it was determined that de/dr for 120-kev protons on Fe_3O_4 was 1.66×10^6 kev/cm and that it varied by only 9% for proton energies between 120 and 60 kev. Using $de/dr' = 1.66 \times 10^6$ kev/cm as the average stopping power over this energy range, equation 8 can be rewritten as

$$\sigma_x = (1.598 \times 10^{-29})\{E_o - (1.66 \times 10^6)r'\}^{3.34}, \qquad (9)$$

where r' is the distance along the proton path in cm, and E_o is the incident proton energy. From this equation it can be determined that σ_x will be reduced to 10% of its initial value when the proton has penetrated approximately 3500 A. Over this depth, the X-ray attenuation factor in equation 2 can be approximated by a linear function as determined, using a computer, from a least-squares fit to the expoential term. The result is

$$\exp(-\mu r') \simeq 0.99 - (13{,}765)r' \qquad (10)$$

where μ was obtained from the tables of Henke (6). The largest deviation between the exponential and linear terms in equation 10 occurs at a depth of 3500 A and is approximately 8.8%. The linear function fits the exponential X-ray attenuation curve with a statistical index of determination of 99.8%. Therefore, for protons incident perpendicular to the sample surface, equation 3 can be approximated by an integral equation of the form

$$I(E_o) = N_o \int_o^T (A - Br')C\left(E_o - \frac{de}{dr'}\right)D \, dr' \qquad (11)$$

where A, B, C, and D are constants determined by computation, de/dr is the stopping power factor, T is the film thickness in cm, and N_o is the concentration of oxygen which, for Fe_3O_4, is 5.38×10^{22} atoms/cm^3. If a non-normally incident proton beam is used, the cos θ factor must be included. This integral equation can be solved in closed form as a function of oxide film thickness, and the result is shown in figure 2 for E_o = 120 kev. Also shown are the values of $I(E_o)$ obtained using the thin-film approximation, equation 7, and the thick-target value of $I(E_o)$ obtained from an extrapolation of Hart's data (5).

The total uncertainty involved in using equation 11 to predict X-ray yields will depend principally on the uncertainties in the values used for σ_x, de/dr', and μ. The systematic error introduced by using a power function to approximate the X-ray attenuation is estimated to be less than ±5%. In the case of Fe_3O_4 presented above, the total uncertainty in the calculated value of $I(E_o)$ is estimated to be ±15%.

From figure 2, it can be seen that (1) the thick-target X-ray yield predicted by solutions of equation 11 and the experimentally measured thick-target yield from Hart differ by only 5%, (2) for film thicknesses where

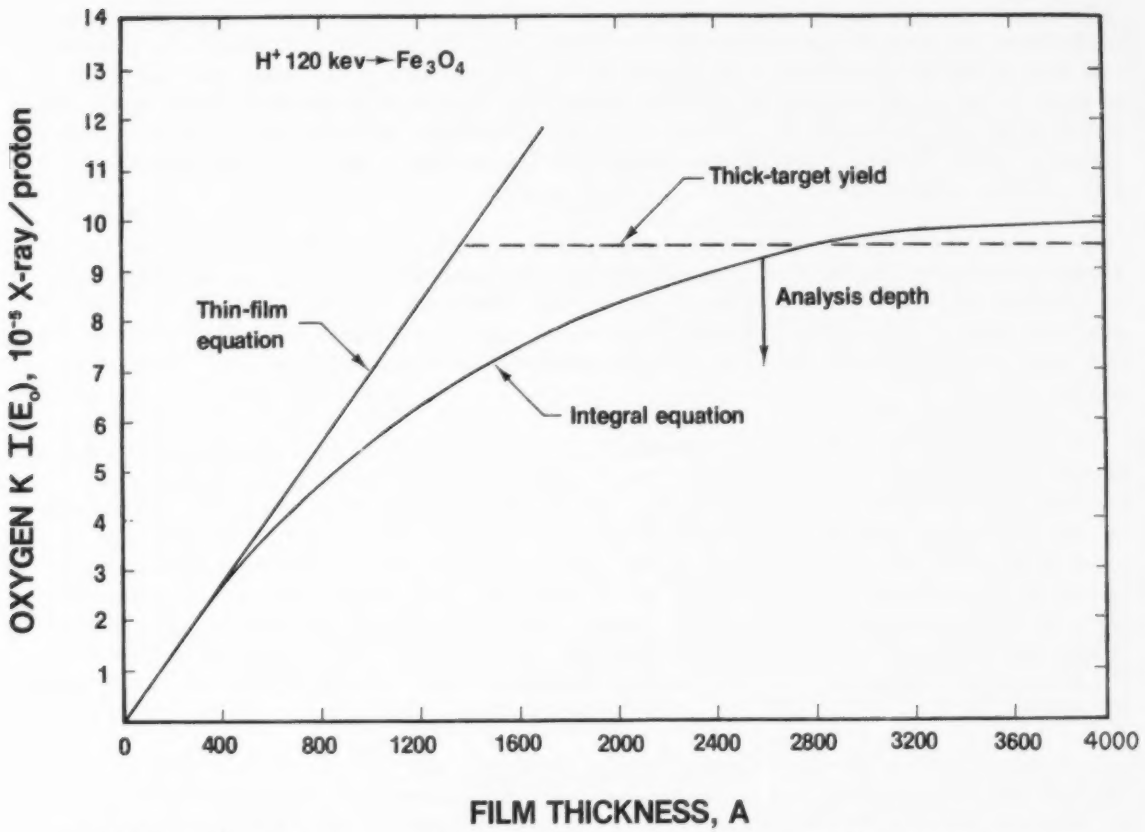

FIGURE 2. - Plot of the oxygen K X-ray yield $I(E_o)$ as a function of Fe_3O_4 film thickness.

proton energy loss becomes significant (greater than ~500 A for Fe_3O_4), the integral equation, rather than the thin-film equation, will be more accurate in determining film thicknesses, and (3) the effective PIXE analysis depth, defined here as that depth at which 90% of the detected X-rays are generated, for 120-kev protons on Fe_3O_4, is approximately 2600 A.

In principle, surface coverages equivalent to small fractions of an atomic layer can be accurately measured using PIXE (9). However, the ultimate practical sensitivity for detecting surface elements is usually limited by the X-ray background originating from the same elements present as bulk impurities within the PIXE analysis depth. In all of the various types of surface studies conducted here, the role of carbon, present as a specific surface impurity on iron, is extremely important. Therefore, the contribution of the "bulk" carbon impurity to the total C K X-ray yield must be known. Using equation 11 with the C K X-ray production cross section as a function of energy (7), the stopping power of protons on iron (2), the absorption of C K X-rays in iron (6), and E_o = 120 kev, the effective analysis depth for a bulk carbon impurity in iron was calculated to be 1100 A. Equation 11 was then evaluated, using T = 1100 A and E_o = 120 kev, for different values of N, the bulk impurity concentration of the carbon. The X-ray yields determined from these

calculations were then inserted into the thin-film equation (equation 7) to calculate the equivalent surface coverage, with the results shown in figure 3. For the studies described here, the bulk carbon impurity level was approximately 50 ppm, as specified by the supplier of the high-purity iron sheet from which the samples were cut. The "signal" (surface carbon) to "noise" (bulk carbon) ratio would, therefore, be 1:1 for a surface carbon coverage of 2×10^{13} carbon atoms/cm^2.

Since the high-purity iron used in the oxidation studies reported here contained approximately 40 ppm oxygen as an impurity, a similar calculation to determine the contribution of this bulk impurity to the measurement of surface oxygen coverages showed that a 1:1 ratio of surface-oxygen signal to bulk-oxygen signal is obtained for a surface coverage of 7×10^{13} oxygen atoms/cm^2.

Although, in principle, equation 11 could be used to determine concentrations of any element in a multielement sample by measuring the X-ray yield and then calculating the factor N_o, this would require an accurate knowledge of the proton stopping power and X-ray absorption for a multielement sample. An alternative method has been used (12) that permits a direct conversion from the experimental X-ray yield, Y, to atomic percent concentration. This method requires the assumption that the target self-absorption of the X-rays can be neglected. Since most of the samples studied in our work consist primarily of 3d transition metals, and since moderately high-energy K-shell X-rays were measured, this assumption has proven to be valid (12).

For a sample whose composition is unknown, the value of Y obtained for each element detected can be normalized using correction factors shown in figure 4, calculated for each K- and L-shell X-ray in the energy range 0.8 to 8.0 kev for protons with an incident energy of 180 kev. The correction factors are the product of the thick-target X-ray yield $I(E_o)$ and the X-ray detection system efficiency for each specific X-ray energy. The quantity of each element is expressed as atomic percent by simply taking the ratio of each normalized value of Y to the sum of the normalized values. This method of calculating concentrations makes the assumption that the solid state detector detects all the elements present in the sample. Since the detector used in this work is limited to X-ray energies greater than 0.8 kev and, therefore, to elements with atomic number greater than 10, the presence of significant quantities of elements such as carbon or oxygen will introduce systematic errors. An example of the use of this method (12) showed excellent results for work on stainless steels.

The use of PIXE with low-energy argon ion sputtering can provide a quantitative method for obtaining either film composition profiles or depth profiles of elements implanted as energetic ions into metal substrates. To obtain the depth profiles of an element, it is only necessary that the PIXE analysis depth be larger than the depth containing that element. Under this condition, a sample can be alternately analyzed to determine the total amount of the element present in atoms per square centimeter using equation 7 or 11 and sputtered using an appropriate low-energy ion beam. A plot of the

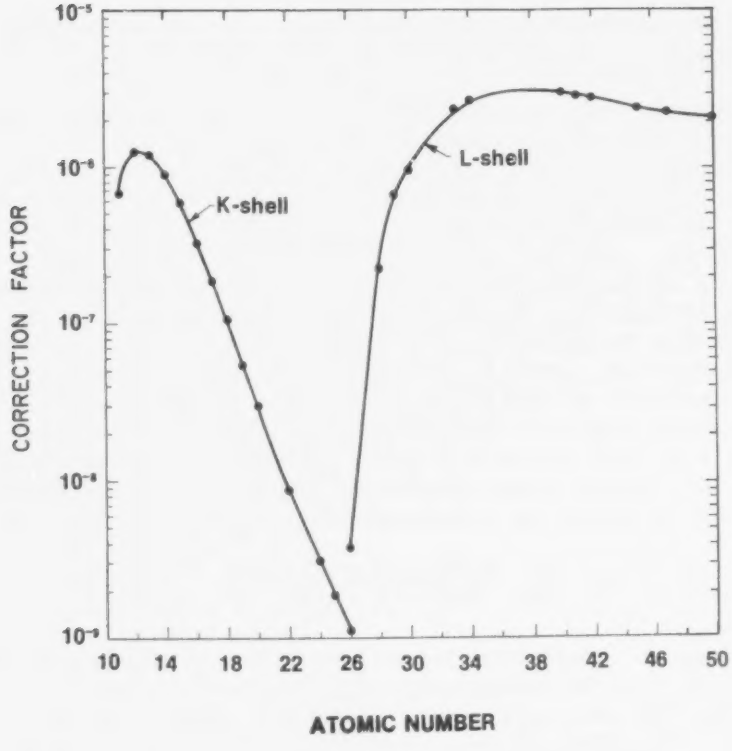

FIGURE 4. - Correction factors used in the normalization of individual X-ray yields to obtain atomic percent concentration for bulk analysis.

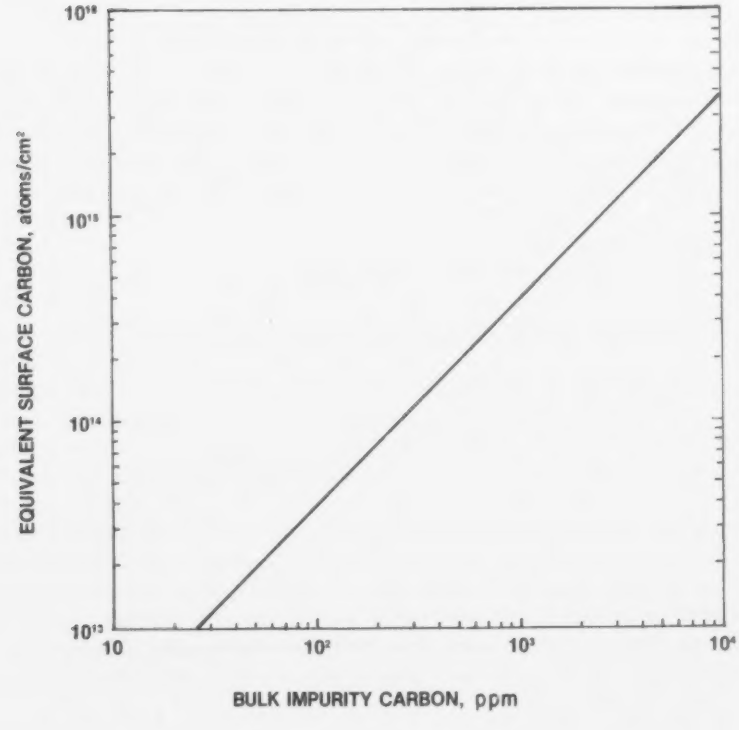

FIGURE 3. - Plot of the equivalent surface coverage of carbon determined by PIXE as a function of the actual bulk carbon impurity concentration.

elemental concentration versus the sputtering charge yields an integral distribution of the element (11).

The sputtering charge can be converted to an equivalent depth in atoms per square centimeter using the equation

$$dN = \frac{dQ(6.25 \times 10^{12})Sf_a}{A_p(1 + \gamma)}, \tag{12}$$

where dN is the amount of the element removed (atoms/cm^2) for a given amount of sputtering charge dQ (μC), A_p is the area of the proton beam on the sample in units of cm^2, γ is the dimensionless secondary electron emission coefficient for the low-energy sputtering ions, f_a is the dimensionless geometrical factor that represents the fraction of the total accumulated sputtering charge Q that is within the proton-beam analysis area, 6.25×10^{12} is the conversion factor from ions to μC, and S is the sputtering yield in atoms/ion. The parameters f_a, A_p, and γ can be determined experimentally. The absolute sputtering yield S can be determined by applying the inversion of equation 12

$$S = \frac{dN}{dQ}\left\{\frac{A_p(1 + \gamma)}{(6.25 \times 10^{12})f_a}\right\} \tag{13}$$

to the PIXE measurements of evaporated thin films of known thickness. For example, a thin film of iron was evaporated onto a chromium substrate. Then the film thickness in atoms per square centimeter was measured as a function of sputtering charge. The slope of this line gave the parameter dN/dQ in equation 13. Since the other parameters in equation 13 are known, the sputtering yield can easily be determined.

Once the sputtering charge has been converted to depth, a smooth curve can be fitted to the integral data points using a least-squares fit, and the curve can then be differentiated to obtain the depth profile in atoms per cubic centimeter plotted as a function of depth. In the next section the results obtained using this technique are presented for iron samples implanted with 25-kev nickel ions.

RESULTS AND DISCUSSION

Cross Sections and Calibration Measurements

The use of either equation 7 or 11 for calculating film thicknesses requires experimental values of the X-ray production cross sections for excitation of inner-shell X-rays. These have been measured in this laboratory for a number of different elements using the procedure described in the review article of Garcia (4). A summary of the K-, L-, and M-shell X-ray production cross sections obtained in this laboratory for 120- and 180-kev proton excitation is presented in figure 5. Where available, data from other laboratories have also been included (5, 7-8, 13). The solid curves are least-squares fits of an exponential function to the data points and permit interpolation to determine cross sections for which there are no experimentally measured values.

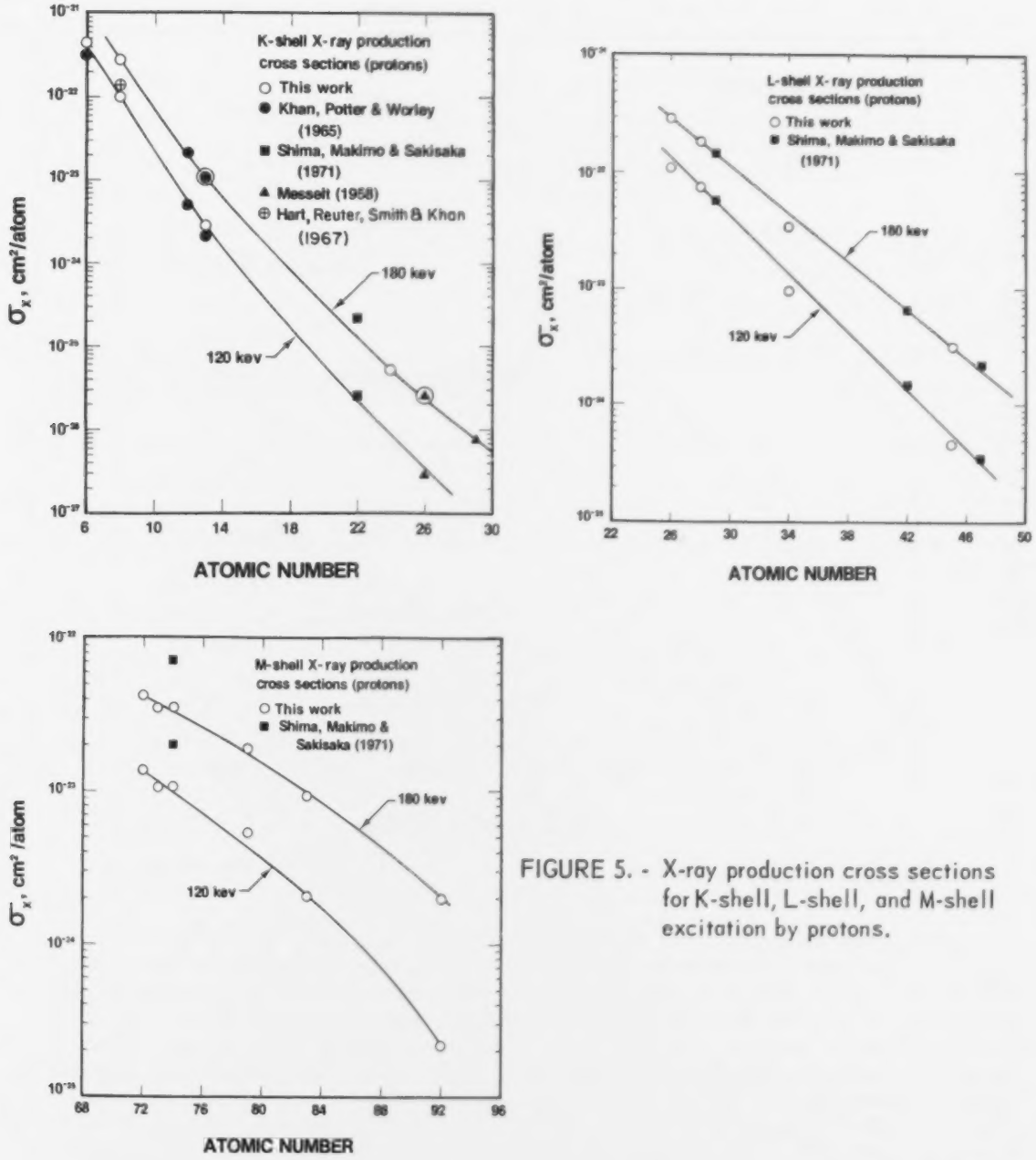

FIGURE 5. - X-ray production cross sections for K-shell, L-shell, and M-shell excitation by protons.

To determine the accuracy of the integral equation 11, a series of calibration experiments was conducted involving the evaporation of iron onto ultra-high-purity (99.999%) aluminum substrates using a tungsten filament evaporator. Using equation 11 with appropriate constants determined by calculation, the experimentally measured Fe L X-ray yield could be related to iron film thickness; the result is shown in figure 6. Prior to evaporation, the

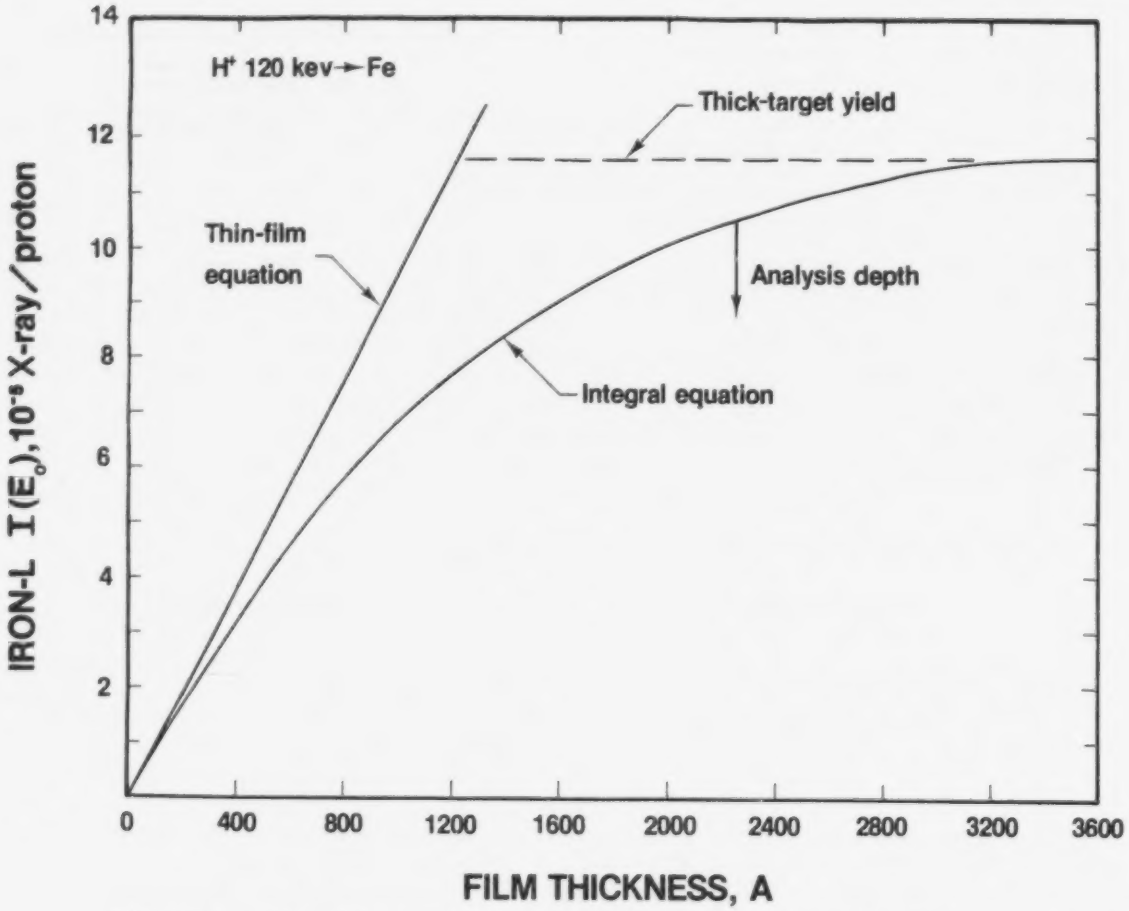

FIGURE 6. - Plot of the iron L X-ray yield as a function of iron film thickness.

Al K yield was measured with 120-kev protons using the gas-flow proportional counter. Various film thicknesses of iron were evaporated onto the aluminum substrates, with the Al K and Fe L yield measured after each evaporation. Using the thin-film (equation 7) and integral approximations (fig. 6), the Fe L yields were used to calculate the thickness of the film in angstroms. From these values, the ratio of the Al K yield after evaporation to the yield before evaporation could be calculated using known values of the stopping power of 120-kev protons in iron (2) and the Al K X-ray attenuation coefficient in iron (6). The predicted ratios for two of these iron film thicknesses are compared with the experimentally measured ratios in table 2. For the thinnest iron film, there was little difference between the thin-film and integral approximation results, and the predicted ratios agree reasonably well with the experimentally measured ratio of 0.54. For the thicker film, since the thin-film approximation neglects proton energy loss and X-ray absorption, the value of 900 A would be expected to be a serious underestimation of the actual film thickness. The integral approximation yields a thickness of

1450 A, a value that predicts an X-ray absorption ratio of 0.18. This compares very well with the experimentally measured ratio of 0.15.

TABLE 2. - Ratio of the substrate aluminum K yields obtained before and after evaporation as compared with the ratio predicted from the evaporated iron film thickness measured using the thin-film and integral approximations

Ratio $(R)^1$ (experimental)	Thin film approximation		Integral approximation	
	Iron thickness, A	Ratio (predicted)	Iron thickness, A	Ratio (predicted)
0.54	411	0.61	500	0.58
0.15	900	.39	1450	.18

$^1R = \frac{\text{Al-K yield after iron evaporation}}{\text{Al-K yield before iron evaporation}}$.

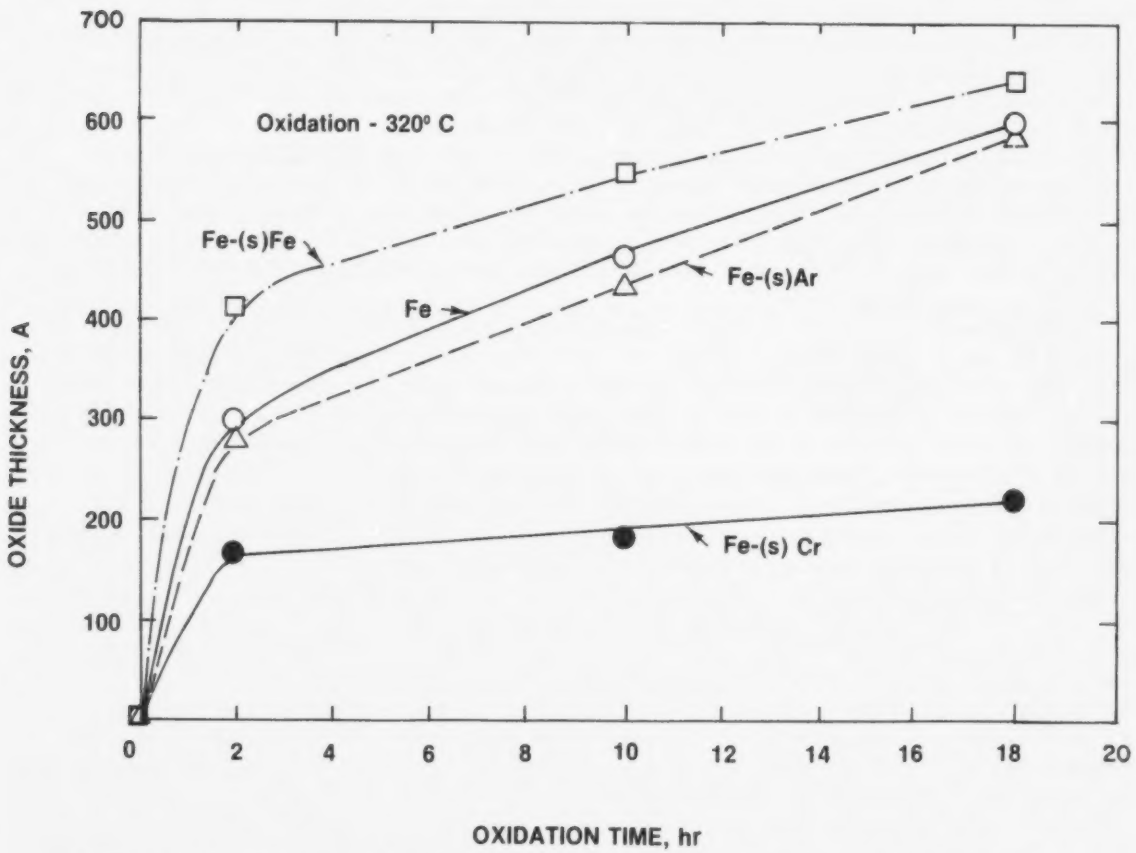

FIGURE 7. - Oxide thickness plotted as a function of exposure time for iron and three ion-implanted iron samples.

Thin-Film Analysis

Proton-induced X-ray emission is an excellent technique for studying the oxidation kinetics of metals and alloys at elevated temperatures. In particular, the effects of certain alloying additions on the oxidation behavior can easily be studied. As an example, figure 7 shows the results obtained using PIXE to determine oxide film thicknesses which illustrate the effects of ion implantation on the oxidation kinetics of iron. Three iron samples were implanted with 3×10^{16} ions/cm^2 of chromium, argon, and iron, respectively, and then oxidized at 320° C in an ambient air environment for times up to 18 hours. The kinetics for the nonimplanted iron and the argon-implanted iron are almost identical, whereas the iron-implanted iron shows an increased initial rate of oxide film formation. The chromium-implanted iron shows a significantly decreased rate of oxidation, which, in fact, is identical to that observed for an Fe-18Cr bulk alloy (10). After the initial 2 hours of oxidation, there was no detectable argon remaining in the argon-implanted iron sample. In this case, the PIXE detection limit was estimated to be 5×10^{14} atoms/cm^2. This result would indicate that the implanted argon probably diffused to the surface where it left it in a gaseous form. Since the implanted iron atoms could not leave the sample in the same manner, the substrate lattice would be expected to recover from the radiation damage at a more rapid rate in the case of the argon implantation. For iron, the disrupted substrate lattice would be in a higher energy state, similar to a grain boundary, and this could account for the increased rate of oxidation. From these studies, it was concluded that the improved oxidation resistance of the Fe-Cr implanted alloy is due not to radiation damage but to the formation of an alloyed region.

To demonstrate the ultimate sensitivity of PIXE for the study of the growth of very thin films, oxidation kinetics were obtained for iron samples with two different preoxidation sulfur surface impurity coverages. The bulk sulfur impurity concentration in the iron samples was 50 ppm, with the different surface coverages obtained using two preoxidation annealing cycles, one of 650° C for 7 minutes and one of 750° C for 20 minutes. Prior to annealing, PIXE analysis using 180-kev protons did not detect any sulfur; indicating that 50 ppm bulk concentration is below the detection limit. However, during annealing, sulfur apparently segregated onto the sulfur, with PIXE analysis indicating a surface coverage of approximately 2×10^{15} atoms/cm^2 for the 650° C annealed sample and approximately 4×10^{15} atoms/cm^2 for the 750° C annealed sample. These two samples were subsequently oxidized at 200° C in an oxygen partial pressure of 2×10^{-6} torr. The results of these experiments are shown in figure 8, where the oxide thicknesses are plottted as a function of the logarithm of exposure time. For the samples with the higher sulfur coverage ($S_1 = 4 \times 10^{15}$ atoms/cm^2), there was an initial induction period during which chemisorption of the oxygen onto the iron surface was retarded, with logarithmic kinetics being observed after 800 seconds of exposure. The sample with the lower preoxidation coverage ($S_1/2 = 2 \times 10^{15}$ atoms/cm^2) exhibited logarithmic kinetics from the beginning of the oxidation cycle. These differences were observed only during the formation of the first few monolayers of the oxide.

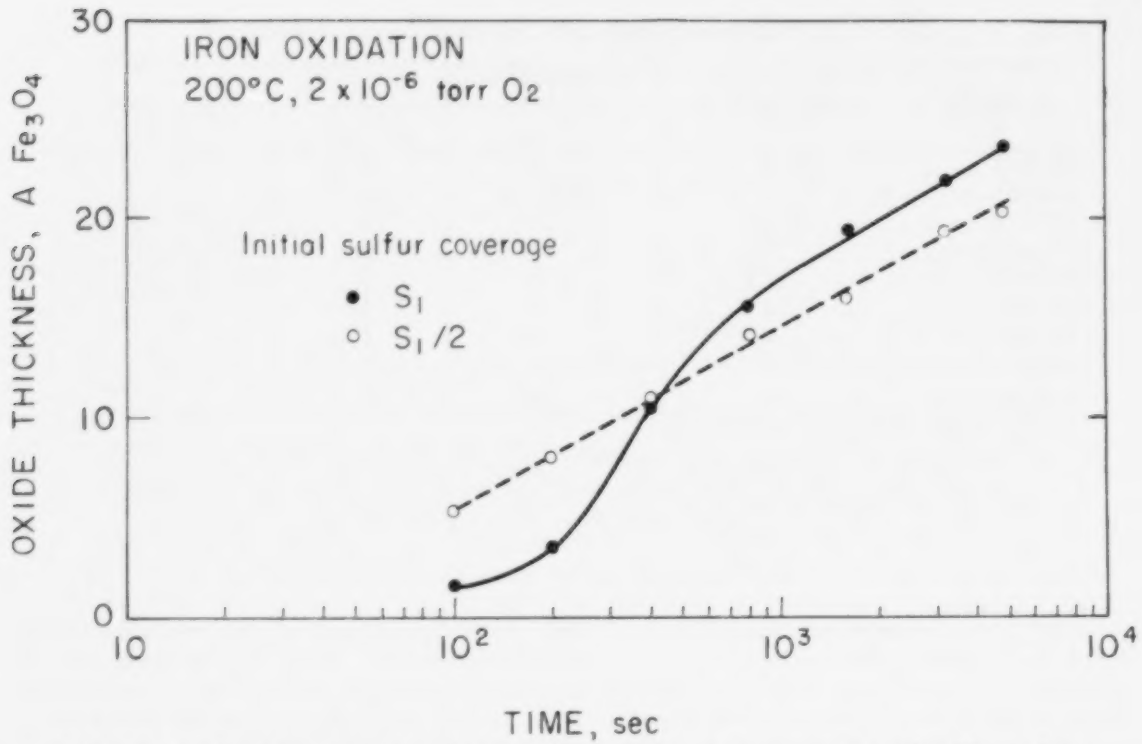

FIGURE 8. - Oxidation kinetics of high-purity iron for two different initial sulfur surface coverages.

Bulk Analysis

An area of corrosion research typical of those for which PIXE has been used for bulk analysis is the study of the redistribution of various alloying elements in power station gas-turbine components that had undergone catastrophic failure. The initial failure occurred at the junction between a nickel-base alloy (Nimonic 105) blade and the iron-base alloy (A-286) wheel. Blade and wheel components were analyzed both at the fracture surface and at an apparently unaffected location several centimeters away. X-ray yields were measured for each element detected, and the concentration of each element (in atomic percent) was calculated by applying the correction factors discussed in the Theory and Applications section. Table 3 summarizes the results for the turbine wheel, showing the changes in the alloy composition at the fracture surface. The results showed that, for the elements initially present in the A-286 alloy, there was a depletion of nickel and chromium but an increase in aluminum and molybdenum in the surface region (≤2500 A) of the wheel at the fracture location. The presence of sodium, chlorine, potassium, and calcium was due to the ocean environment near the power station, and salts of these elements could have been involved in the processes that led to the initiation of the fracture.

TABLE 3. - PIXE results for the A-286 turbine wheel

Element	A-286 alloy,[1] at. pct	Nonfracture region, at. pct	Fracture region, at. pct	Change,[2] pct (fracture region)
Nickel.....	25.1	21.5	12.2	-51
Chromium....	16.3	16.5	13.1	-20
Iron.....	54.0	56.7	56.3	0
Aluminum....	.52	.21	1.5	+188
Molybdenum..	.73	1.10	3.0	+310
Calcium.....	.0	.27	1.9	+
Potassium...	.0	.32	2.0	+
Chlorine....	.0	.0	2.0	+
Sodium.....	.0	.0	2.4	+

[1] Data from Handbook of Metals (1).

[2] The changes are listed with respect to the Handbook values since the changes that led to the failure could have proceeded to a lesser degree in the nonfracture system. The uncertainty in these calculations is estimated at ±10%, and the percentage changes were considered to be zero if the calculated changes were less than ±10%.

Table 4 summarizes the PIXE analyses of two portions of the turbine blade. For the elements initially present in the Nimonic-105 alloy, there were decreases in chromium, cobalt, aluminum, and molybdenum in the fraction region. There were also decreases in the concentration of molybdenum and aluminum at a point 3 cm from the fracture. Since data provided with the turbine components indicated that they originally met the Handbook specifications, this depletion away from the fracture was believed to be due to a corrosion process in which compounds of molybdenum and aluminum were formed as corrosion products, with a resultant depletion of these elements near the surface. Another possible explanation would be that the molybdenum and aluminum diffused from the turbine blade to the wheel since the concentrations of these elements increased near the fracture region on the wheel, as indicated in table 3. Since the turbine blade initially contained only 1.5% iron, the large increase in the concentration of that element was probably due to its presence as a corrosion product from the turbine wheel or diffusion into the blade from the iron-base turbine wheel.

TABLE 4. - PIXE results for the Nimonic-105 blade

Element	Nimonic-105[1] alloy, at. pct	3 cm from fracture region, at. pct	Fracture region, at. pct	Change,[2] pct (fracture region)
Molybdenum..	2.8	0.6	0.09	-97
Aluminum....	9.6	3.6	.70	-93
Chromium....	15.7	18.8	9.1	-24
Cobalt.....	19.1	20.8	10.4	-45
Nickel.....	48.4	52.6	52.1	0
Iron.....	1.0	.0	25.4	+2,440
Potassium...	.0	.56	.28	+
Chlorine....	.0	.0	.34	+
Calcium.....	.0	.58	.50	+

[1] Data from Handbook of Metals (1).

[2] The changes are listed with respect to the Handbook values since the changes that led to the failure could have proceeded to a lesser degree in the nonfracture system. The uncertainty in these calculations is estimated at ±10%, and the percentage changes were considered to be zero if the calculated changes were less than ±10%.

The results obtained by PIXE for both the turbine blade and wheel contributed to the conclusion by the power company that corrosion fatigue failure was initiated in the turbine wheel. The initial fracture subsequently proceeded to a degree where failure occurred and the turbine blade could no longer be supported.

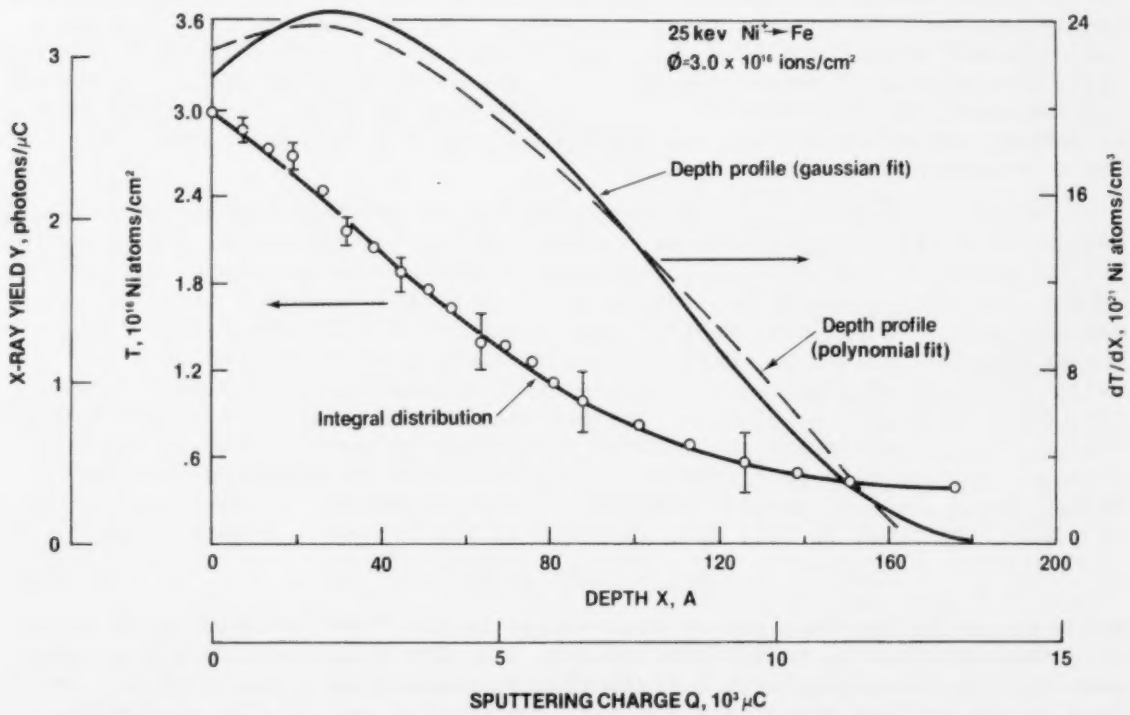

FIGURE 9. - Integral distribution and depth profiles as determined by the PIXE-sputtering technique for 25-kev Ni^+ implantation into iron.

Depth Profiling

The PIXE-ion sputtering technique has been applied extensively to determining the alloy concentration as a function of depth for alloys formed by ion implantation. For the example presented here, polycrystalline iron was implanted with 25 kev Ni^+ to a total fluence, ϕ, of 3×10^{16} ions/cm^2. Figure 9 demonstrates how the profile was obtained. The data points, which constitute the integral profile, are initially plotted as the experimental X-ray yield, Y, expressed as detected Ni K X-rays per microcoulomb of 180-kev protons, as a function of measured accumulated sputtering charge of 1.0-kev argon ions. Next, the abscissa is converted to a depth scale using equation 12, with S = 4.1 atoms/ion as measured in a separate experiment in this laboratory. Since most of the implanted nickel was within 160 A of the surface, the thin-film equation could be used to determine the number of atoms per square centimeter of nickel in the substrate. Using equations 1 and 7, the experimental X-ray yield was converted to T, the number of nickel atoms per square centimeter. It should be noted that, in the derivation of equation 7, T represented a film thickness; however, in this usage, it now represents implanted atoms per square centimeter.

Two types of smooth curves were fit to the data points, the first being a fourth-order polynomial and the second being the integral of a gaussian function (11). Only one curve is shown in the figure since the two fitted curves could not be resolved in the figure. Differentiating these two curves gives dT/dx, the absolute concentration of nickel as a function of depth. These two profiles, shown in figure 9, are in excellent agreement. Since the currently accepted theory describing the energy loss of high-velocity ions in solids predicts that the ions will come to rest in a gaussianlike distribution (11), the gaussian fit was used to obtain the depth profiles for all types of ion-implanted alloys. However, for the more general case of an element with an unknown distribution near the surface of a sample, the polynomial fit would be more appropriate.

Figure 10 represents the integral profile of an electrodeposited platinum coating on an Fe-5Cr substrate as analyzed with 150-kev protons. To determine the thickness of the coating, the integral approximation can be used. However, at the time this analysis was taken, the Pt M X-ray production cross section was not known. Therefore, another method was devised for accurately determining the film thickness which utilizes estimates of the effect of a particular thickness of platinum on the experimental yield of Fe K X-rays originating from the Fe-5Cr substrate. The estimate assumes a sharp boundary between the coating and substrate and ignores the effect of the chromium in the substrate. Initially, a pure iron sample was analyzed to determine the experimental X-ray yield at several different proton energies. A least-squares fit of a power function to this data resulted in the following relationship:

$$Y_{Fe\ K} = (1.90 \times 10^{-13})E_o^{\ 6} \qquad (14)$$

where E_o is the incident proton beam energy in kev. For example, at E_o = 150 kev, the experimental Fe K X-ray yield is 2.2 For a sample with a platinum coating, the experimental Fe K yield will be reduced as a result of (1) energy loss of the protons traversing the platinum coating and (2) the absorption of the Fe K X-rays in the coating. Assuming a constant proton stopping power in

the platinum of 0.02 kev/A (2), the proton energy at the interface between the coating and substrate is given by $E = E_o - 0.02t$, where t is the coating thickness in A. Using the mass absorption coefficient of Fe K X-rays in platinum (14), the absorption can be expressed as $\exp(-7.72 \times 10^{-5})t$. Therefore, the experimental Fe K X-ray yield that will be measured for a platinum coating of thickness t on an iron substrate will be given by the equation.

$$Y_{Fe\ K} = (1.90 \times 10^{-13})(E_o - 0.02t)^6 \exp\{(-7.72 \times 10^{-5})t\}. \qquad (15)$$

Equation 15 was solved for various values of t to give the best manual fit to the Fe K data points of figure 10. The best fit was obtained for a platinum coating thickness of 1650 A, assuming an interface at 4.0×10^2 mC of sputtering. Therefore, it is possible to determine film or coating thickness indirectly by measuring the X-ray yield for the substrate.

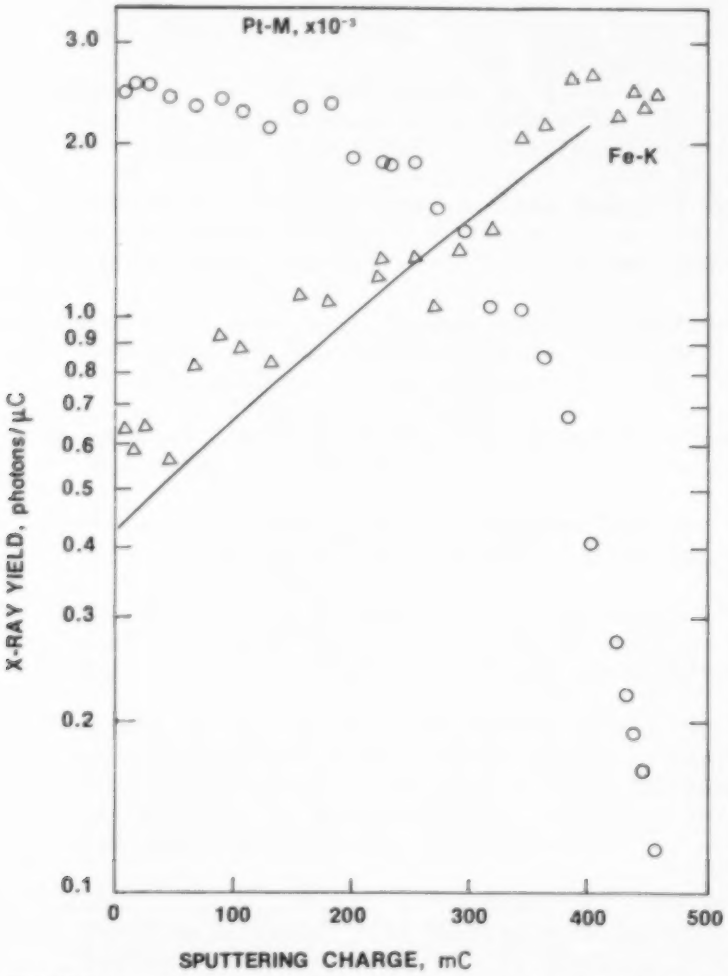

FIGURE 10. - Platinum M and iron K experimental X-ray yields for 150-kev proton bombardment as a function of sputtering charge for an electrodeposited platinum film.

SUMMARY AND CONCLUSIONS

The PIXE and PIXE-sputtering techniques are very useful methods for determining the concentrations and depth profiles of elements present in the near-surface regions of solids. An integral approximation to the general equation for the X-ray yield due to proton impact provides an accurate means of determining film thicknesses up to several thousand angstroms. This equation has also been used to determine the contribution of bulk impurity X-rays to the PIXE analysis of surfaces and thin films. The sensitivity of PIXE for the measurement of very-thin-film growth kinetics has been demonstrated from studies of the effect of submonolayer coverages of sulfur on the initial oxidation kinetics of polycrystalline iron.

Results have been presented to show the use of PIXE to determine bulk alloy composition changes caused by corrosion fatigue. These analyses contributed to the determination of which elements were responsible for the failure and showed that there was a redistribution of some of the alloying elements at the fracture surface.

Finally, PIXE combined with low-energy argon ion sputtering has been used to obtain quantitative depth profiles of nickel-implanted polycrystalline iron. By measuring the sputtering yield, the depth profiles can be obtained in terms of the absolute concentration of the implanted element as a function of depth.

REFERENCES

1. American Society for Metals. Handbook of Metals. Metals Park, Ohio, 1961, 8th ed., 650 pp.

2. Andersen, H. H., and J. F. Ziegler. Hydrogen Stopping Powers and Ranges in All Elements. Pergamon Press, New York, 1977, 317 pp.

3. Christensen, L. J., and J. M. Khan, and W. F. Brunner. Measurements of Microgram Surface Densities by Observation of Proton-Produced X-Rays. Rev. Sci. Instr., v. 38, January 1967, pp. 20-24.

4. Garcia, J. D., R. J. Fortner, and T. M. Kavanagh. Inner Shell Vacancy Production in Ion-Atom Collisions. Rev. Modern Phys., v. 45, July 1973, pp. 111-162.

5. Hart, R. R., F. W. Reuter III, H. P. Smith, Jr., and J. M. Khan. Oxygen K-Shell X-Ray Production in Thin Films of Aluminum Oxide by 20- to 100-kev Protons. Phys. Rev., v. 179, March 1967, pp. 4-9.

6. Henke, B. L., and E. S. Ebisu. Low Energy X-Ray and Electron Absorption Within Solids (100-1500 eV Region). Ch. in Advances in X-Ray Analysis, Plenum Press, New York, v. 17, 1974, pp. 150-213.

7. Khan, J. M., and D. L. Potter, and R. D. Worley. Studies in X-Ray Production by Proton Bombardment. Phys. Rev., v. 139, October 1965, pp. A1735-A1746.

8. Messelt, S. K-Shell Ionization by Protons. Nuclear Physics, v. 5, July 1958, pp. 436-446.

9. Musket, R. G., and W. Bauer. Surface Analysis Using Proton Beams. Thin Solid Films, v. 19, January 1973, pp. 69-74.

10. Sartwell, B. D., A. B. Campbell III, B. S. Covino, Jr., and T. J. Driscoll. Applications of Ion Implantation to Metallic Corrosion. Trans. Nuclear Sci., v. NS-26, February 1979, pp. 1670-1676.

11. Sartwell, B. D., A. B. Campbell III, and P. B. Needham, Jr. Formation of Corrosion-Resistant Surface Alloys by Implantation of Low-Energy Nickel.and Chromium Ions Into Polycrystalline Iron. Ch. in Ion Implantation in Semiconductors, ed. by F. Chernow. Plenum Press, New York, 1977, pp. 201-211.

12. Sartwell, B. D., and P. B. Needham, Jr. The Use of Proton-Excited X-Ray Emission To Study: (1) Electrodeposited TiB_2 Coatings and (2) Gas-Turbine Blade Failures. Ch. in Advances in X-Ray Analysis, ed. by R. W. Gould, C. S. Barrett, J. B. Newkirk, and C. O. Ruud. Plenum Press, New York, v. 19, 1976, pp. 293-303.

13. Shima, K., I. Makimo, and M. Sakisaka. Proton-Induced K-, L-, and M-Shell X-Ray Production Cross Sections. J. Phys. Soc. Japan, v. 30, October 1971, pp. 611-616.

14. Stainer, H. M. X-Ray Mass Absorption Coefficients. A Literature Survey. BuMines IC 8166, 1963, 124 pp.

☆U.S. GOVERNMENT PRINTING OFFICE: 1980-603-102/72

INT.-BU.OF MINES,PGH.,PA. 24641